Evidence of the disorder-independent electron-phonon scattering time in thin NbN films

A. I. Lomakin,[1,2] E. M. Baeva,[1,2] A. D. Triznova,[2] N. A. Titova,[2] P. I. Zolotov,[2,3] A. V. Semenov,[2] D. E. Sunegin,[4] A. V. Lubenchenko,[5] A. I. Kolbatova,[1,2,*] and G. N. Goltsman[1,6]

[1]*National Research University Higher School of Economics, 20 Myasnitskaya St, Moscow 101000, Russia*
[2]*Moscow Pedagogical State University, 29 Malaya Pirogovskaya St, Moscow 119435, Russia*
[3]*LLC Superconducting Nanotechnology (SCONTEL), 11A Derbenevskaya Naberezhnaya, Moscow 115114, Russia*
[4]*Osipyan Institute of Solid State Physics RAS (ISSP RAS), 2 Academician Osipyan St, Chernogolovka, Moscow District 142432, Russia*
[5]*National Research University MPEI, 14 Krasnokazarmennaya St, Moscow 111250, Russia*
[6]*Russian Quantum Center, 100 Novaya Street, Skolkovo, Moscow 143025, Russia*

(Received 8 July 2022; revised 5 February 2023; accepted 9 February 2023; published 24 February 2023)

We report on experimental study of the effect of disorder on electronic parameters and inelastic scattering mechanisms in ultrathin superconducting NbN films, which are commonly used in single-photon detectors. An increase in disorder in the studied 2.5-nm-thick NbN films characterized by Ioffe-Regel parameter from 6.3 to 1.6 is accompanied by a decrease in the critical temperature T_c from 11.5 to 3.4 K. By measuring magnetoconductance in the range from T_c to $\sim 3T_c$, we extract the inelastic scattering rates of electrons, including electron-phonon (e-ph) scattering rate $\tau_{\text{e-ph}}^{-1}$. We observe that $\tau_{\text{e-ph}}^{-1}$ and their temperature dependencies are insensitive to disorder that is not described by the existing models of the e-ph scattering in disordered metals. As temperature decreases, the temperature dependence of $\tau_{\text{e-ph}}^{-1}$ varies from T^3 to T^2, which can be result of a decrease in the dimensionality of phonons involved in the e-ph scattering process. Our results call for further theoretical and experimental studies of the e-ph scattering in ultrathin disordered films.

DOI: 10.1103/PhysRevB.107.054205

I. INTRODUCTION

Physical mechanisms governing superconducting and electronic properties of ultrathin films have been studied extensively in order to understand the impact of disorder and quantum effects on electron transport in that sort of materials [1]. Despite its fundamental importance, these studies are also motivated by usability of thin disordered films in nanoscale superconducting devices, such as photon detectors [2–5]. To optimize the operation of these thin-film devices, it is essential to know parameters, which control the nonequilibrium response to radiation: for instance, electronic and phonon heat capacities, electron diffusivity, rates of inelastic electron-electron (e-e) and electron-phonon (e-ph) scattering processes. Numerous studies of electron transport in disordered metals reveal significant impact of disorder on mechanisms of inelastic scattering. For example, an enhancement of the e-e scattering rates is expected due to a strong elastic scattering of quasiparticles in thin disordered films [6] or due to presence of a moderate density of magnetic impurities [7,8]. It is also proposed that strong disorder can modify the e-ph scattering, and one can expect weakening or strengthening of the e-ph interaction, depending on the specific properties of disordered systems [9,10], or emergence of additional relaxation channels [11]. In samples with reduced dimensions, relaxation processes also depend on sample size [12–14], which can lead to an even greater variety of effects in inelastic relaxation. Thus, understanding a role of disorder in inelastic scattering in thin-film devices can come mainly from an empirical study of a specific material.

Thin film of niobium nitride (NbN) is a typical material, in which disorder can be tuned from moderate to strong limit [15–17]. This material has been extensively used for production of modern electronic devices such as SNSPDs (superconducting nanowire single-photon detectors) [18,19], HEB (hot electron bolometer) mixers [20], microwave nanoinductors [21] and resonators [22], quantum phase-slip devices [23–28], etc. The choice of NbN for these technological applications has been justified by its relatively high superconducting critical temperature ($T_c \approx$ 10–12 K in ($d \approx 5$)-nm-thick films), high values of resistivity ($\rho > 100\ \mu\Omega\,\text{cm}$) and the relatively fast e-ph relaxation ($\tau_{\text{e-ph}} \sim 10$ ps at $T_c \approx 10$ K [29]). On the fundamental level there is observed an ongoing interest in effects of disorder on superconducting and normal-state properties in NbN films [15,16,30–34]. Mechanisms of inelastic relaxation in thin NbN films have been studied with various experimental methods, however, significant inconsistencies in the data have appeared in literature over the past decades [29,35–40]. They are mainly caused by changing material parameters due to different deposition conditions. Nevertheless, a steady progress in production of NbN films [17,41,42] opens up new horizons for further research, in particular for a systematic study of the effect of disorder on electron transport and inelastic scattering in ultrathin films of NbN.

In this work we have prepared a set of ultrathin NbN samples with a tunable intrinsic disorder by depositing films in different conditions. Here we change only one deposition parameter at a time and fix the others. We studied evolution

*Corresponding author: kardakova@rplab.ru

TABLE I. Parameters of NbN films.

№	$R_s^{300\,\mathrm{K}}$ (Ω/sq)	r_R	$k_F l$	T_c (K)	D (cm^2/s)	$\xi_{\mathrm{GL}}(0)$ (nm)	$B_{c2}(0)$ (T)	$n \times 10^{29}$ (m^{-3})	τ (fs)	l (Å)	$N_0 \times 10^{28}$ (eV^{-1} m^{-3})	R_{NS} (Ω/sq)	$\tau_{\text{e-ph}}(T_c)$ (ps)	p	ε_F (eV)
s1	437	0.85	6.3	11.54	0.59	3.9	14.8	1.9	0.7	3.5	4.8	497	8.3	3.05	5.9
s2	509	0.81	5.5	10.76	0.57	4.0	14.3	1.8	0.6	3.16	4.3	602	7	3	6.2
s3	815	0.72	3.5	8.43	0.36	3.6	17.9	1.7	0.4	2	4.3	1010	20.5	3.05	5.9
s4	912	0.69	3.2	7.02	0.35	3.8	15.3	1.6	0.35	1.9	3.9	1160	21	2.4	6.1
s5	1025	0.67	2.8	6.03	0.34	4.1	13.5	1.6	0.27	1.65	3.6	1287	20	2	6.6
s6	1574	0.38	2.1	3.40	0.27	4.9	9.7	1	0.28	1.5	3.0	2550	30	1.7	5.0
s7	1950	0.26	1.6		0.19			1.1	0.15	1.1	2.4		300 ($T = 1$ K)	1.7	6.9

of electronic parameters and inelastic scattering mechanisms with the increase of disorder. To study inelastic scattering we applied magnetoconductance measurements, which have been successfully used to study inelastic scattering in some samples of NbN [39,43] and NbTiN [44] recently. We have observed that the increase of disorder in the studied NbN films has no noticeable effect on the magnitude and the temperature dependence of the e-ph scattering rate $\tau_{\text{e-ph}}^{-1}$. The results for $\tau_{\text{e-ph}}^{-1}$ are also in good agreement with previous experimental data, extracted from the magnetoconductance for NbN films [39] as well as with the results obtained from a photoresponse of the NbN detector [29].

II. SAMPLES AND MEASUREMENT SETUP

Ultrathin NbN films are deposited using magnetron sputtering system (AJA International Inc.) with a background pressure of 9×10^{-8} torr. Samples are deposited on r-cut sapphire substrates by sputtering of Nb target in an argon-nitrogen atmosphere (99.998% purity of both gases). Growth rate equal to 0.065 nm/s is controlled via quartz crystal microbalance in each deposition run. Studied films have thickness of $d = 2.5$ nm. The level of disorder in five NbN films (s1–s5 in Table I) is varied by changing a substrate temperature in each deposition process T_{dep}: 500 °C, 400 °C, 300 °C, 150 °C, and 25 °C (no additional heating), respectively. The films s1–s5 are also grown at a fixed nitrogen concentration of 22%, while operating pressure is maintained constant at 3.6 mtorr. Heating of substrates was carried out by using the built-in resistive SiC heater with a PID controller. The most disordered samples are grown at the following conditions: $T_{\text{dep}} = 500$ °C; 27% of nitrogen at 6.5 mtorr for s6 and 23% of nitrogen at 6.8 mtorr for s7. Operating pressure was adjusted using a throttle valve. As result, we obtained NbN films of the same thickness but of different resistance per square R_s and critical temperature T_c by varying heating of substrates and partial nitrogen pressure. To prevent unintentional oxidation of NbN films in the atmosphere, films are covered with a 5-nm-thick passivating silicon layer *in situ*. Structural characterization of a 2.5-nm-thick NbN sample (s1) is performed using x-ray diffraction analysis, x-ray photoelectron spectroscopy (XPS), and atomic force microscopy (AFM). The details of structural characterization are given in Appendix A.

To study transport properties of NbN, we patterned films into 500-μm-wide and 1000-μm-long Hall bars. Electrical transport measurements were carried out with Lake Shore 370 AC Resistance Bridge at a bias current less than 1 μA. Normal-state resistance R_s was measured in a four-probe configuration. The measurements were carried out in a homemade ^{4}He cryogenic insert immersed in a dewar and performed in a wide temperature range (from 300 to 1.7 K). At low temperatures we measured magnetoresistance $R_s(B)$, temperature dependencies of the second critical magnetic field $B_{c2}(T)$ and the Hall constant $R_H^{25\,\mathrm{K}}$ at 25 K by applying perpendicular magnetic field B up to 4 T. By measuring $R(T)$ dependencies at different values of B (not shown here) we determined the slope dB_{c2}/dT at T_c. The latter allows to estimate the critical magnetic field $B_{c2}(0)$, the electron diffusivity D, and the Ginzburg-Landau (GL) coherence length $\xi_{\mathrm{GL}}(0)$ using the following expressions: $B_{c2}(0) = -0.69T_c(dB_{c2}/dT)$, $D = -4k_B/(\pi e)(dB_{c2}/dT)^{-1}$, and $\xi_{\mathrm{GL}}^2(0) = \pi\hbar D/(8k_B T_c)$. Here, the critical temperature T_c is determined as temperature at $R_s = R_{\max}/2$.

III. RESULTS AND DISCUSSION

A. Normal-state properties

Figure 1 shows temperature dependencies of the sheet resistance R_s for all NbN films under study. R_s for all films

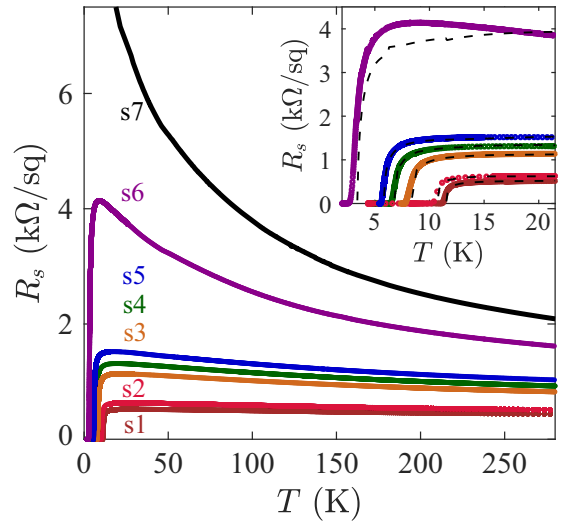

FIG. 1. Temperature dependencies of the sheet resistance $R_s(T)$ for all samples (main panel) and only for superconducting samples (s1–s6) in the narrow temperature range near their superconducting transitions (inset). The dashed lines represent fits obtained from the quantum corrections to conductivity taking into account superconducting fluctuations, weak localization, and e-e interaction (see text for details).

gradually rises as temperature decreases and drops to zero at vicinity of T_c. The temperature trend of R_s can be characterized by the resistance ratio parameter $r_R = R_s^{300\,\mathrm{K}}/R_{\max}$, where $R_{\max}$ is the maximal sheet resistance just above the resistive transition. Commonly observed $r_R < 1$ is well-known behavior for disordered NbN films. It reflects sensitivity of electron system to quantum corrections, meanwhile contribution of e-ph scattering is considered to be negligible here. We also observed the suppression of T_c with increasing disorder, which is consistent with the fermionic mechanism of suppression of superconductivity in moderately disordered films (see Appendix B for details).

Table I gives an overview of metallic properties for studied NbN films. The details about the carrier density n, the Ioffe-Regel (disorder) parameter $k_F l$, the mean-free path l, the electron diffusivity D, and the density of states N_0 estimates are provided in Appendix C. High normal-state resistance R_s and low resistance ratio parameter r_R of the magnetron-sputtered NbN films are also known to be influenced by the grain-boundary scattering [45–47]. One should note that the graininess of ultrathin NbN films is not as pronounced as that of thick films (see AFM studies of ultrathin NbN films in Appendix A). Meanwhile, we assume that the electron transport through the grains can be considered as a factor limiting the mean-free path in NbN films.

B. Magnetoconductance

To study inelastic relaxation in NbN films as a function of disorder, we measured magnetoresistance by varying magnetic field B in the range from 0 to 4 T at a set of fixed temperatures from T_c to 30 K. The NbN films studied represent quasi-two-dimensional (2D) system with respect to characteristic length scales, i.e., the thermal coherence length $L_T = \sqrt{\hbar D/k_B T}$ and the superconducting coherence length ξ_{GL} ($d < \xi_{\mathrm{GL}}, L_T$). The dimensionless change in magnetoconductance at the fixed T can be determined from the measured $R_s(B, T)$ using the following expression:

$$\delta G(B, T) = \frac{2\pi^2\hbar}{e^2}[R_s(B, T)^{-1} - R_s(0, T)^{-1}]. \qquad (1)$$

Figure 2 shows typical experimental dependencies of $\delta G(B, T)$ for NbN samples. The data, presented for a representative sample (s5), look similar for other samples.

Applying the fluctuation spectroscopy approach, we fit the experimental data in Fig. 2 by the relative magnetoconductance δG^{QC} (see the Appendix D for details). In this approach δG^{QC} for superconducting samples reflects the change in conductance originated from superconducting fluctuations and the weak localization. Using T_c as a fitting parameter, we estimated the anomalous Maki-Thompson term, which contains information about the temperature-dependent electron phase-breaking rate $\tau_\phi^{-1}(T)$. Note that the choice of T_c in 2D disordered superconducting films is ambiguous due to disorder-induced spatial inhomogeneity of superconducting properties [48–50]. Nevertheless, in our measurements the choice of T_c barely affects the extracted values of $\tau_\phi(T)$ (see Appendix E for details). The best fits of $\delta G(B, T)$ in Fig. 2 are shown with black curves with values of T_c varying in under 2% in respect to the values determined at $R_s = R_{\max}/2$. It is important to note that the phase-breaking length $L_\phi = \sqrt{D\tau_\phi}$ is larger than the film thickness d in a considered temperature range. This fact supports validity of using 2D expressions for NbN films under study. The values of $\tau_\phi(T)$, obtained for the most disordered and nonsuperconducting sample (s7), are extracted by taking into account only the weak localization term [see Eq. (D1a) in the Appendix D].

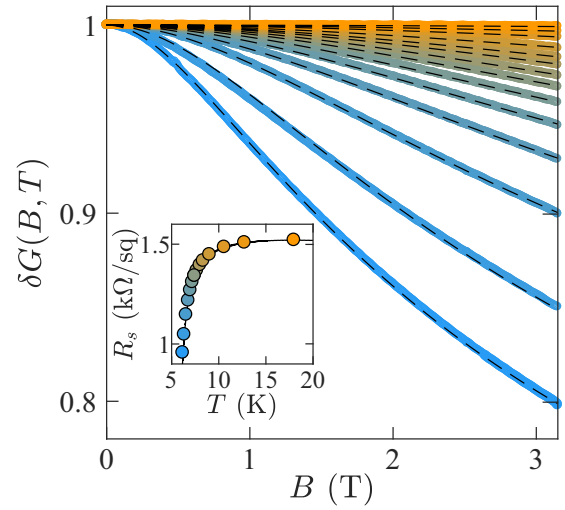

FIG. 2. Experimental dependencies of the normalized magnetoconductance $\delta G(B, T)$ for a representative sample (s5). Different colors of the curves correspond to different operating temperatures marked on the $R_s(T)$ curve in the inset. The dashed black curves represent fits by Eq. (D1).

The same approach, with adding the e-e scattering term to the conductivity, can be exploited for fitting of $R_s(T)$ dependencies above T_c (see the inset of Fig. 1). Here we use the expression $R_s(T) = 1/[R_{NS}^{-1} + e^2/(2\pi^2\hbar)G^{\mathrm{QC}}(0, T)]$, where R_{NS} is a fitting parameter and the values of τ_ϕ in $G^{\mathrm{QC}}(0, T)$ are those extracted from the magnetoconductance processing. The values of R_{NS} turn out to be close to $R_s^{300\,\mathrm{K}}$ for moderately disordered films. The discrepancy between $R_s^{300\,\mathrm{K}}$ and R_{NS} in the strongly disordered NbN film (s6) may be explained by changing their granular properties (size of granules, intergranular properties) and approaching the Anderson-Mott transition [51].

C. Electron phase-breaking rate

As a next step, we explore the impact of disorder on inelastic scattering in NbN films. Figure 3(a) shows the temperature dependencies of τ_ϕ^{-1} for all studied samples. First of all, the data demonstrate the close resemblance of the results for NbN samples with different level of disorder. The data are characterized by close values of τ_ϕ^{-1}, as well as a similar power-law decrease in τ_ϕ^{-1} with lowering temperature. The exact expression for τ_ϕ^{-1} is represented by sum of scattering mechanisms due to superconducting fluctuations $\tau_{\mathrm{e\text{-}fl}}^{-1}$, the e-e scattering rate $\tau_{\mathrm{e\text{-}e}}^{-1}$, the spin-flip scattering rate τ_s^{-1}, and the e-ph scattering rate $\tau_{\mathrm{e\text{-}ph}}^{-1}$ as follows [52]:

$$\tau_\phi^{-1}(T) = \tau_{\mathrm{e\text{-}fl}}^{-1} + \tau_{\mathrm{e\text{-}e}}^{-1} + \tau_s^{-1} + \tau_{\mathrm{e\text{-}ph}}^{-1}. \qquad (2)$$

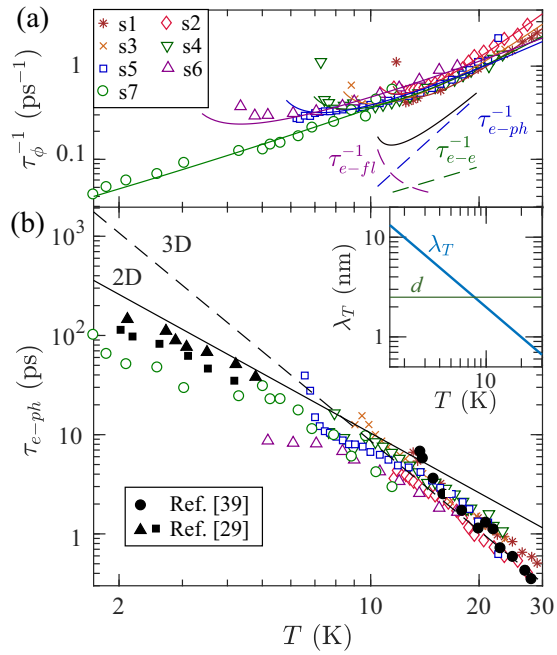

FIG. 3. Temperature dependencies of (a) the electron dephasing rate τ_ϕ^{-1} extracted from magnetoconductance measurements and (b) the e-ph scattering time $\tau_{\text{e-ph}}$ extracted from τ_ϕ^{-1}. The data are plotted in symbols on a log-log scale. In (a) the solid curves show the best fits of τ_ϕ^{-1} by Eq. (2). The inset in (a) shows a schematic layout for the fit by Eq. (2), where the solid line is the sum of the scattering mechanisms, the dashed lines are the contributions of the e-ph, e-e, and SC dephasing mechanisms. In (b) the solid and dashed lines demonstrate predictions for the e-ph scattering on three-dimensional (3D) and two-dimensional (2D) phonons, respectively, with the power-law dependencies $\propto T^{-3}$ and $\propto T^{-2}$ in clean case. The inset in (b) presents the temperature dependence of the phonon wavelength and its comparison with thickness of NbN films studied in this work.

The presence of surface magnetic defects can significantly increase τ_ϕ^{-1} [7,8] and lead to the T-independent behavior at low temperatures [8,13]. The magnetic disorder in superconductors can lead to a time-reversal symmetry breaking caused by spin-flip scattering, altering superconducting state and suppressing T_c more strongly than the nonmagnetic disorder [53–55]. Recent studies of Nb and NbN-based devices reveal unintentional surface magnetic disorder due to the unpaired spins in native oxide [56–59]. Nevertheless, we found that the passivating Si layer on top of NbN films fortunately prevented strong oxidation (see XPS analysis in Appendix A). In addition, the suppression of T_c in our films can be explained by the strong electron interaction (see Appendix B). Thus, we treat the effects of magnetic disorder as negligible in analysis of τ_ϕ^{-1} dependencies.

The e-e and superconducting fluctuations phase-breaking rates can be defined as [6,60]

$$\tau_{\text{e-fl}}^{-1} = \frac{\pi g k_B T}{\hbar} \frac{2 \ln 2}{\epsilon + \beta}, \tag{2a}$$

$$\tau_{\text{e-e}}^{-1} = \frac{\pi g k_B T}{\hbar} \ln\left(\frac{1}{2\pi g}\right), \tag{2b}$$

where $\beta = 4 \ln 2/\{\sqrt{\ln^2[1/(2\pi g)] + 64/(\pi^2 g)} + \ln(2\pi g)\}$, $g = e^2 R_s^{300\,\text{K}}/(2\pi^2\hbar)$ and $\epsilon = \ln(T/T_c)$. The value of $R_s^{300\,\text{K}}$ is taken here at the highest temperature of our measurements (300 K), where the effect of e-e interactions is expected to be small [51,61]. The expression for the e-e scattering rate accounts only for the processes with small energy transfer, the so-called Nyquist quasielastic scattering, which dominates in our experimental temperature range with $T < \hbar/(k_B\tau) \sim 10^3$ K. The e-e scattering rate is expected to enhance greatly with increasing disorder [6], but we estimate the increase of $\tau_{\text{e-e}}^{-1}$ as two times for the given change of $R_s^{300\,\text{K}}$. Since τ_ϕ^{-1} in our measurements is characterized by a stronger T dependence than the e-e and SC phase-breaking rates, we believe that the e-ph scattering is the dominant dephasing process here. Applying that $\tau_{\text{e-ph}} = \alpha_{\text{e-ph}}^{-1}(T/T_c)^p$, where p and $\alpha_{\text{e-ph}}$ are fitting constants, we fit the data in Fig. 3(a) (see the dashed lines). Table I gives an overview of the best-fit values for the power index p and $\alpha_{\text{e-ph}} = \tau_{\text{e-ph}}(T_c)$, where the latter reflects the e-ph scattering time at T_c.

Figure 3(b) shows the temperature dependencies of $\tau_{\text{e-ph}}$ extracted from the total dephasing rate τ_ϕ^{-1} by subtracting $\tau_{\text{e-e}}^{-1}$ and $\tau_{\text{e-fl}}^{-1}$. We observe that the magnitude and the temperature dependencies of $\tau_{\text{e-ph}}$ for the studied NbN films do not depend on disorder, but demonstrate the nonmonotonic temperature dependence: it is proportional to T^{-3} above 10 K, and it modifies to T^{-2} at lower temperatures. To compare our findings with the previous results, we added to Fig. 3(b) the experimental data for some different NbN films measured by magnetoconductance in Ref. [39] and extracted from a response to the amplitude-modulated radiation (AMAR method) of NbN detector in Refs. [29,62]. We observe the close agreement between all experimental data for $\tau_{\text{e-ph}}$ obtained for various NbN films. Below we will discuss potential mechanisms responsible for the observed rates of the e-ph scattering.

D. Electron-phonon scattering in ultrathin films

In search of potential explanation for the observed τ_ϕ^{-1} behavior, we turned to the existing models of the e-ph scattering in thin disordered metals [9,63,64]. In general, the e-ph coupling occurs because the passing phonons distort the local lattice structure and conduction electrons respond to the resulting band distortion. A widely used standard model of the low-temperature e-ph scattering in bulk metals (i.e., jellium model) [65,66] assumes (i) a clean three-dimensional (3D) free-electron gas with a spherical Fermi surface; (ii) a Debye description of the acoustic phonons; (iii) the scalar deformation potential, expected to be dominant at long-wavelength phonons; and (iv) the dimensions of the metal are much longer than the average phonon wavelength (3D phonon spectrum). In this model, the average e-ph scattering rate appropriate for these assumptions is given by [65,66]: $\tau_{\text{e-ph}}^{-1} = [6\zeta(3)(k_B T)^3(2\varepsilon_F/3)^2]/[2\pi\rho_m\Omega\hbar^4 u_s^4 v_F]$, where $\hbar$ is the reduced Planck's constant, ρ_m the mass density, Ω the metal volume, u_s the sound speed, v_F the Fermi velocity, and $\varepsilon_F = 3n/(2N_0)$ the Fermi energy. In disordered metals the e-ph scattering is nonlocal with a characteristic size of the interaction region about the phonon wavelength λ_T.

The impact of disorder on the e-ph coupling is controlled by the product $q_T l$, where $q_T = k_B T/\hbar u_s$ is the wave vector of the thermal phonon. In the disordered metals with $q_T l < 1$, the theory considers the following modifications of the rate $\tau_{\text{e-ph}}^{-1} \propto T^4 l$ [9,63,64] and $\tau_{\text{e-ph}}^{-1} \propto T^2 l^{-1}$ [10], depending on the dominant phonon polarization (longitudinal or transverse ones) and type of disorder (vibrating or static types). One should note that numerous studies of the inelastic scattering with magnetoconductance reveal that there does not exist a universal temperature behavior of $\tau_{\text{e-ph}}^{-1}$ in disordered conductors [13]. In particular, the value of the temperature exponent p might be quite sensitive to the microscopic quality and the intrinsic material properties such as characteristic of the Fermi surface [67,68], the dimensionality of the electron and phonon systems [69], nontrivial phonon dispersion [70], etc.

Study of the inelastic scattering with magnetoconductance in NbN films reveals that the power-law index p and the magnitude of $\tau_{\text{e-ph}}^{-1}$ do not change with increasing disorder in an explicit way. Note that the spread of the estimated values of the Fermi energy (see Table I) is within 10%, so in the further analysis, we assume that the change in the electronic parameters makes a negligible contribution to the change in the e-ph scattering. On the other hand, one would expect that $\tau_{\text{e-ph}}^{-1}$ strongly depends on the phonon properties, which, in samples with reduced dimensions, may differ from the Debye spectrum, accepted in the models. Previous studies of the response of thin NbN films to the modulated terahertz radiation revealed a $T^{1.6}$ dependence of the e-ph relaxation rate [29] [see the black-filled symbols in Fig. 3(b)], which has been explained by the renormalization of the phonon spectrum in thin films.

In this work, we compare the experimental data in Fig. 3(b) with the theoretical predictions for the e-ph scattering in clean case ($q_T l > 1$). One can describe the electron scattering on 3D phonons by the expression $\tau_{\text{e-ph, 3D}}^{-1} = [7\pi\zeta(3)\lambda_{3D} k_B T^3)/(2\hbar\theta_{D,3D}^2]$ [71], and for 2D phonons by $\tau_{\text{e-ph, 2D}}^{-1} = \lambda_{2D} k_B T^2/(\hbar\theta_{D,2d} D)$. Here λ is the e-ph coupling constant, $\theta_{D,3D} = \hbar(6\pi^2)^{1/3} u_{3D}/(a k_B)$ and $u_{3D} = [1/3(2/u_t^3 + 1/u_l^3)]^{-1/3}$, $\theta_{D,2D} = \hbar(4\pi)^{1/2} u_{2D}/(a k_B)$, and $u_{2D} = [1/2(1/u_t^2 + 1/u_l^2)]^{-1/2}$ are the Debye temperatures and the mean sound velocities, respectively, for 3D and 2D phonons, $a = 0.44$ nm is the NbN lattice constant. The fitting values $\lambda_{3D} = 0.98$ (the same value as in Ref. [72]), $\theta_{D,3D} = 116$ K with $u_{3D} = 1.73 \times 10^3$ m/s for 3D case and $\lambda_{2D} = 1$, $\theta_{D,2D} = 118$ K with $u_{2D} = 1.93 \times 10^3$ m/s for 2D case provide the close agreement with the experimental data in Fig. 3(b). Note that the fitting value of $\theta_{D,3D}$ is a few times less than Debye temperatures reported for bulk NbN (735 K [73]), but it is typical for the values reported for thin films ($\theta_D \sim$ 172–174 K) [15,39]. Taking into account the average value of u_m, one can estimate the phonon wavelength $\lambda_T = h u_m/(2.82 k_B T)$ (here 2.82 is a constant given in the dominant phonon approximation), which is comparable with the film thickness d [see the inset of Fig. 3(b)]. Here the crossover $\lambda_T \approx d$ is expected at $T_{cr} \approx 10$ K. Therefore, the e-ph scattering in ultrathin NbN films can be considered in 3D regime at temperatures higher than T_{cr}, and in 2D regime at low temperatures.

To ensure the condition that the film is two dimensional for the phonons, one can assume that there is a substantial acoustic mismatch between the film and and the substrate [74,75]. In that case, the quantization of the phonon spectrum in direction perpendicular to the film may be significant, leading to reduced phonon density of states and, hence, a weakened temperature dependence. Using the fitting parameters $\theta_D = 116$ K, $u_m = 1.73 \times 10^3$ m/s, and the value of the phonon escape time $\tau_{\text{esc}} = 120$ ps (see Appendix F for details), we estimate the phonon transmission coefficient $\eta = 4d/(\tau_{\text{esc}} u_m) \approx 0.05$, which is consistent with the previous results for NbN/Al_2O_3 interface [39]. This small value of η indicates that available directions for the phonon escape from the ultrathin film are strongly restricted.

Another surprising fact is that the observed T dependencies of $\tau_{\text{e-ph}}$ for NbN films are close to predictions of the simple model for the e-ph scattering in clean metals. In our study, we observe a significant increase of the sheet resistance with change of deposition conditions, which may indicate a change in microstructure properties. Meanwhile, the impact of disorder on the e-ph coupling, which falls into the range $0.26 \leqslant q_T l \leqslant 0.80$ and $0.08 \leqslant q_T l \leqslant 0.25$ at $10 < T < 30$ K for s1 and s7, respectively, corresponds to weakly disordered regime (here we take $u_m = 1.73 \times 10^3$ m/s for the estimate). We also see that the disorder weakly affects the e-ph scattering rates in these NbN films. One should note that the disorder in the models of the e-ph scattering [9,10,13] is usually treated as point defects, while in NbN films the increase in resistance and decrease in the mean-free path may be related to a different origin, for instance, electron tunneling through thin grain boundaries. Thus, the disorder-independent character of $\tau_{\text{e-ph}}^{-1}$ in granular samples might come from presence of weakly disordered metal grains with the T dependencies mainly determined by the phonon spectrum. One can assume that the phonon wavelength will be greater than the characteristic scale of grain boundaries, so the phonons are unlikely to sense these barriers. However, this assumption requires further theoretical and empirical study.

IV. DISCUSSION

In this paper, we investigate the evolution of electronic parameters and inelastic scattering rates with increasing disorder in ultrathin NbN films. We find that the inelastic scattering rates of electrons and their temperature dependencies are close for NbN films of different microscopic quality and with different levels of disorder. Our experimental results in Fig. 3 are in agreement with previous studies of the inelastic scattering times in NbN films [29,39].

One should note that, in detectors, the energy relaxation time due to e-ph scattering $\tau_{\text{E-PH}}$ differ from $\tau_{\text{e-ph}}$ by a numerical coefficient $\tau_{\text{E-PH}} = \alpha \tau_{\text{e-ph}}$, where $\alpha \approx 0.6$–0.1 for $p = 2$–4, respectively [76]. Thus, the weak dependence on disorder for $\tau_{\text{e-ph}}(T_c)$ in NbN films with a higher level of disorder and lower T_c values can facilitate for increase of sensitivity and spectral characteristics of HEBs devices [3] as well as for increase the efficiency of single-photon detection of SNSPDs. In the latter case, the fast inelastic scattering and the electron diffusivity both affect the hot-spot size and the superconducting gap suppression [77]. This expectation

correlates with a recent breakthrough in detection efficiency in SNSPDs, when one uses NbN films with high normal-state resistance values [17,78,79]. On the other hand, one should keep in mind that the operation of the detectors is also limited by the phonon escape rate, which is proportional to the sound velocity. As shown in Appendix D, the analysis of $\tau_{\text{e-ph}}^{-1}(T)$ dependence indicates low values of the sound velocity, which in turn can affect the phonon escape rate and limit the device response. Thus, further experimental study of the features of phonon transport in ultrathin disordered metals is advisable.

In summary, we observe the disorder-independent character of the electron-phonon scattering time in ultrathin NbN films. The observed results are not described by existing models of the e-ph scattering in disordered metals. The experimental values of $\tau_{\text{e-ph}}^{-1}$, measured above 10 K, are proportional to T^3, expected for the electron scattering on three-dimensional acoustic phonons in clean case. At lower temperatures, $\tau_{\text{e-ph}}^{-1}$ modifies to T^2, which is likely due to lowering the dimensionality of the phonons involved in the e-ph scattering. Our results call for further theoretical and experimental studies of the e-ph scattering in thin disordered films, in particular, in the case when the disorder is caused by a granular microstructure.

ACKNOWLEDGMENTS

We acknowledge valuable discussions with V. S. Khrapai and M. Sidorova. We are grateful to S. V. Simonov for their assistance with the x-ray studies. X-ray studies were performed using Rigaku SmartLab SE diffractometer at shared facility center of ISSP RAS. The growth of NbN films, material characterization, and magnetotransport measurements were funded by the RFBR Project No. 19-32-60076. The surface analysis and analysis of transport properties were carried out with the financial support of the Ministry of Science and Higher Education of the Russian Federation in the framework of the Agreement No. 075-11-2022-026.

APPENDIX A: X-RAY DIFFRACTION, XPS ANALYSIS, AND ATOMIC FORCE MICROSCOPY OF A NBN FILM

Structural characterization of a 2.5-nm-thick NbN sample (s1) is shown in Fig. 4. We plot the x-ray diffraction (XRD) data for a coupled $\omega - 2\theta$ scan and identify main diffraction peaks of NbN (101), (202) and Al_2O_3 (012), (024) for film and for substrate, respectively. The x-ray data indicate that NbN_x has a tetragonal phase (γ phase), which is generally characterized by $x = 0.75$–0.84 [80]. This phase is considered to be a deformed cubic phase (δ phase) with a similar transition temperature and the electronic spectrum as in a δ phase but has less N content [81,82]. The observed γ phase is in accordance with the phase diagram of NbN calculated as a function of the substrate heating temperature [83].

Figure 5 displays the experimental data on x-ray photoelectron spectroscopy (XPS) presented for the least-disordered sample in the set (s1). The XPS studies of sample surfaces were performed with the help of the electron-ion spectroscopy module based on Nanofab 25 (NT-MDT) platform in the analysis chamber an ultrahigh oil-free vacuum about 10^{-6} Pa.

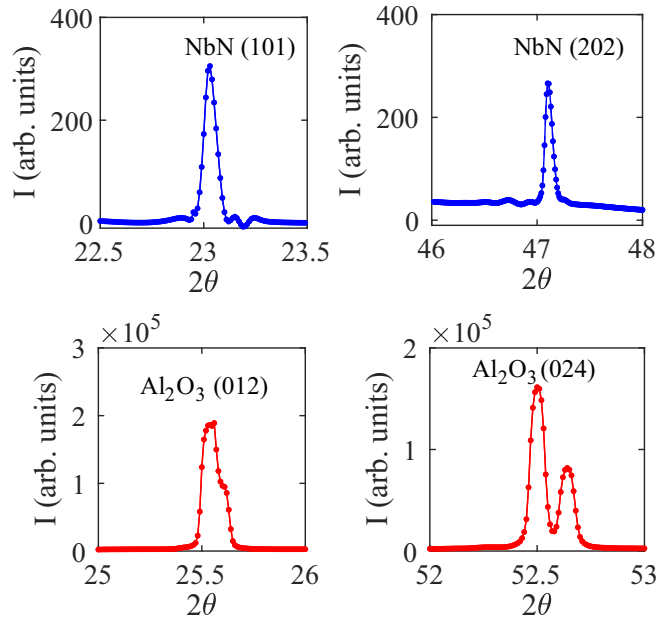

FIG. 4. X-ray diffraction study of NbN sample (s1). Coupled $\omega - 2\theta$ scan, obtained with a RIGAKU diffractometer using Cu$K\alpha 1$ source ($\lambda = 1.540\,59$ Å). The positions of diffraction peaks with the corresponding diffraction angles are the following: (a) 23.03°, NbN (101); (b) 47.01°, NbN(202); (c) 25.55°, Al_2O_3 (012); and (d) 52.57°, Al_2O_3 (024). The XRD data indicate that the studied sample has a tetragonal phase (γ phase) with the space group *I-4m2*.

Figure 5 shows decomposition of XPS lines of an element of interest (Nb, N, O, Al) into component peaks that reveal presence of different phases in the sample (NbN_x, NbN-Si).The XPS results are obtained on the base of the method described in Ref. [84]. The results allow to extract thicknesses of layers of different phases. The data for the studied NbN sample are presented in Table II.

Figure 6 shows the atomic force microscope (AFM) images of a few NbN samples covered by 5-nm-thick Si layer and a sapphire substrate. The AFM images are obtained with NT-MDT (INTEGRA series) setup in classical contact mode. The rms surface roughness of NbN films is below 0.2 nm, which corresponds to atomically smooth surface. In contrast to thick NbN films ($d > 10$ nm), which have a pronounced granular structure [85], ultrathin NbN can be considered as a quasiamorphous matrix with the grain size smaller the film thickness.

Surface topography of NbN_x is known to be strongly affected by the substrate heating temperature T_{dep} and the nitrogen partial pressure during deposition process [86]. As shown in Fig. 6, the microstructure of the samples deposited at high T_{dep} (s1, s6) is compact grained since heating of the substrate increases mobility of adatoms and increases density of the film. The sample deposited at room temperature (s5) is characterized by less compact microstructure without pronounced grains. As the nitrogen content in the system changed, various and interrelated types of crystallographic structures are expected to form [83,86]. With increase of the nitrogen background pressure, one can expect that the kinetic energy and flux of the ablated materials are reduced, and the

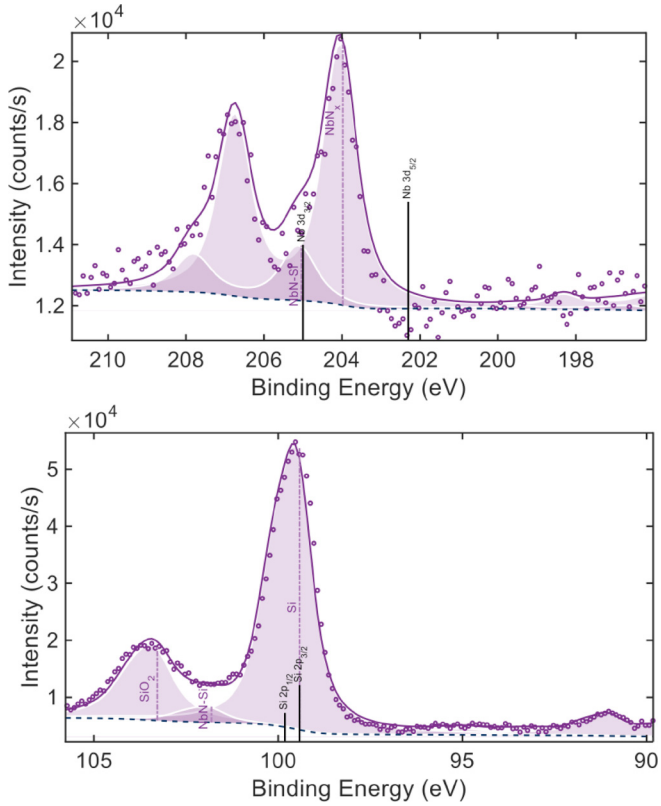

FIG. 5. XPS spectra of NbN sample (s1). The detailed scans of strong lines: lines Nb 3d (top figure) and lines Si 2p (bottom figure). The circles show the recorded detailed spectra, the solid lines are calculated using method described in Ref. [84], the area shows separate calculated peaks.

latter results in less nitrogen ratio in NbN_x film as well as a decrease in material density [80].

APPENDIX B: VARIATION OF T_c IN ULTRATHIN NBN FILMS

Here we discuss the correlation between T_c and $k_F l$, shown in Fig. 7. The breakdown of the superconductivity with the increase of disorder can be related to two different, but not mutually exclusive effects [1]. The first effect results from a decrease of electronic screening, which enhances the e-e repulsion and partially cancels the e-ph mediated attractive interaction. This fermionic effect leads to a mechanism described in Refs. [87,88]. The second effect comes from the disorder-induced decrease in superfluid density, which makes

TABLE II. Chemical and phase depth profile of the ultrathin NbN film (s1).

	Formula	d (nm)
1	SiO_2	1.03 ± 0.19
2	Si	5.3 ± 0.5
3	NbN-Si	0.59 ± 0.11
4	NbN	not records
Substrate	Al_2O_3	Inf

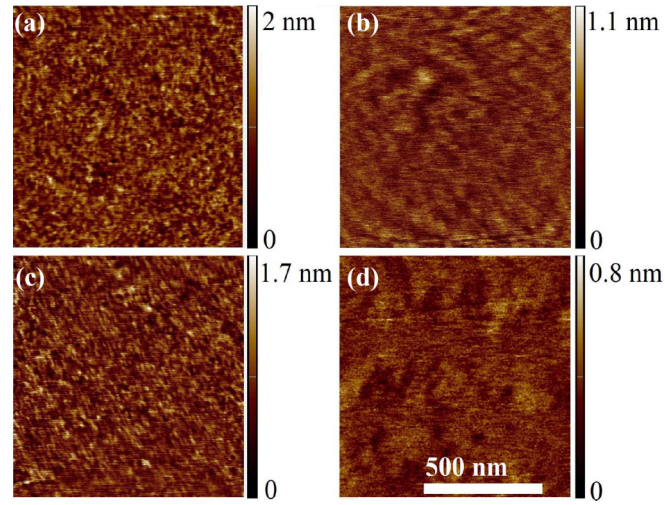

FIG. 6. AFM images of representative NbN samples and a substrate: (a) s1, (b) s5, (c) s6, (d) r-cut sapphire. The rms roughness of the samples (s1, s5, s6) and the substrate are 0.20, 0.13, 0.19, and 0.06 nm, respectively.

a superconductor susceptible to phase fluctuations [89,90]. The latter is known as a bosonic mechanism.

As shown in Fig. 7, the suppression of T_c follows the expectations of the fermionic mechanism, which can be expressed in the following form [88]:

$$\frac{T_{c0} - T_c}{T_{c0}} = \frac{\alpha_{3D}}{k_F l} + \frac{\lambda_{e\text{-}e}}{2(k_F l)(k_F d)} \ln^3 \frac{\hbar}{T_{c0}\tau_D}, \qquad \text{(B1)}$$

where the first term in the right-hand side corresponds to the three-dimensional ballistic motion of electrons, the second term in the right-hand side is related to 2D diffusive motion of electrons. Here T_{c0} is the critical temperature in bulk, $\lambda_{e\text{-}e}$ is the electron-electron coupling constant, and α_{3D} is the material-dependent coefficient of the order of unity. The experimental data are in good agreement with Eq. (B1)

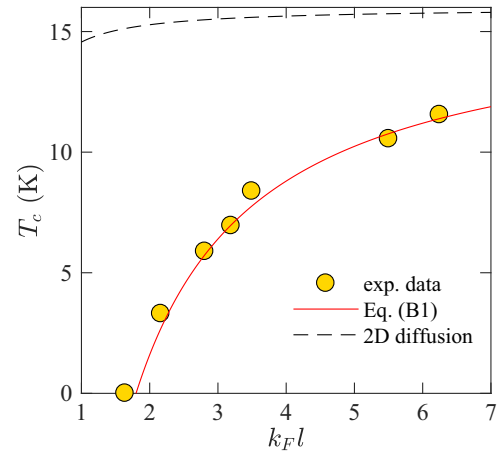

FIG. 7. Suppression of the critical temperature T_c with disorder. The experimental data (symbols) are in comparison with the fermionic mechanism of T_c suppression (see the red solid line). The contribution of the 2D diffusion motion of electrons in Eq. (B1) is shown by the black dashed line.

taking $\lambda_{e\text{-}e} = \frac{1}{2}$, $k_F = 1.6 \times 10^{10}$ m^{-1}, $\tau_D = 40$ fs, and treating $T_{c0} = 16$ K and $\alpha_{3D} = 1.8$ as the fitting parameters (see the red solid line in Fig. 7). It is instructive to note that suppression of T_c, related to 2D diffusive nature of electron motion, is weak here (the black dashed line), and it is likely determined by the 3D ballistics [88]. The observed dependence can be associated with the following hierarchy of length scales $l \ll d \simeq \xi$ in the studied NbN films, and thus the suppression of T_c is likely to be controlled by $k_F l$ parameter rather than R_s. One should also note that the change in the density of states at the Fermi level is small (see values of N_0 in Table I) and cannot distort the analysis within the framework of the fermionic scenario.

Meanwhile, in the previous studies [16,30], the electronic system in NbN films was observed to undergo the fermionic scenario at moderate level of disorder ($k_F l > 3$) and cross to a bosonic route at stronger disorder ($k_F l < 3$). The estimated level of disorder in our NbN films, in comparison to those in Ref. [16], shows that the e-e repulsion can play a major role in destruction of the superconducting state for samples s1–s5, whereas the strong phase fluctuations due to small superfluid density can be more pronounced for the most disordered samples in this study (s6 and s7). The latter means that these two effects, which provide the disorder-induced suppression of T_c, should be considered collectively. However, we leave further refinements beyond the scope of this work since the exact microscopic picture of the suppression of T_c does not play a large role in the results obtained for $\tau_\phi(T)$ (see Appendix E for details).

APPENDIX C: ELECTRON TRANSPORT

We calculate all electronic parameters at the highest temperature of our measurements (300 K), where the effect of e-e interactions is expected to be small [61]. First, to estimate the Hall coefficient $R_H^{300\,\mathrm{K}}$ we consider the expression $(R_H^{25\,\mathrm{K}} - R_H^{300\,\mathrm{K}})/R_H^{300\,\mathrm{K}} = \gamma(R_s^{25\,\mathrm{K}} - R_s^{300\,\mathrm{K}})/R_s^{300\,\mathrm{K}}$ [6], where $\gamma = 0.68$ is an empirical parameter [91]. Using the value of $R_H^{300\,\mathrm{K}}$ we derive the carrier density $n = -B/(edR_H^{300\,\mathrm{K}})$, where e is the electron charge. It is also important to note that samples s1–s5 are characterized by a moderate change (<20 %) in the carrier density n at increase of $R_s^{300\,\mathrm{K}}$ in two times. Meanwhile, the most disordered samples (s6 and s7) are characterized by a twofold decrease of n at threefold and fourfold increase of $R_s^{300\,\mathrm{K}}$. The latter change in n can be a result of the increase of Nb and N vacancies due to the increase of the nitrogen partial pressure in the mixture during deposition of NbN [15].

To characterize electron transport, we estimate the mean-free path (mfp) l, the elastic scattering time τ, and the single-spin density of states (DOS) at the Fermi level N_0 assuming the free-electron model [92] and using the expressions $l = \hbar k_F/(e^2 n R_s^{300\,\mathrm{K}} d)$, $\tau = l^2/3D$, and $N_0 = 1/(2R_s^{300\,\mathrm{K}} d e^2 D)$, where $k_F = (3\pi^2 n)^{1/3}$ is the Fermi wave vector. We believe that this *ab initio* estimates are well justified since $l \approx 1$–3.5 Å, which is in order of the lattice constant in our disordered NbN films, thereby a possible Fermi-surface anisotropy can be negligible. The electronic transport is also characterized by the Ioffe-Regel parameter $k_F l$, which is a common indicator of the disorder in homogeneously disordered material. All estimated parameters are listed in Table I.

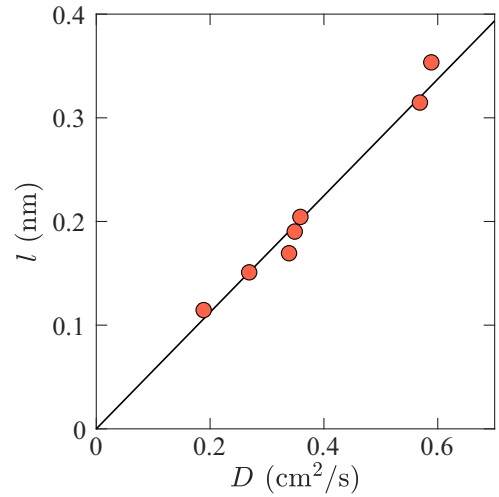

FIG. 8. Electron transport in the normal state. The relationship of the electron diffusivity D and the mean-free path l. The solid line shows the approximation with $l = 3D/v_F$, where $v_F \approx (5.3 \pm 0.3) \times 10^5$ m/s.

In addition, Fig. 8 shows the relationship between the experimental values of l and D, which can be approximated as $l = 3D/v_F$, where $v_F \approx (5.3 \pm 0.3) \times 10^5$ m/s is the Fermi velocity determined as a fitting parameter here. The estimate of v_F is two times lower than the one previously reported [32], and it corresponds to the effective mass of charge carriers $m_{\mathrm{eff}} = \hbar k_F/v_F$, which decreases from $4.1m_e$ to $3.3m_e$ as $R_s^{300\,\mathrm{K}}$ increases (here m_e is the mass of a free electron). Note that taking into account these values of m_{eff} allows to correct underestimation of n determined from optical measurements in NbN [93].

We would also like to note one more feature of electron transport in NbN. Typical estimates of the mfp obtained in the experiment turned out to be smaller than the lattice constant ($a \approx 0.44$ nm [72,94]). This indicates that, in addition to scattering by point defects, the mfp can be significantly affected by another mechanism, for example, scattering by grain boundaries [95]. Thick NbN films are known to exhibit a pronounced polycrystalline structure [85], while ultrathin NbN films are rather a quasiamorphous matrix with randomly oriented grains. In this case, the grain size is expected to be smaller than the film thickness but larger than the characteristic unit cell. In a simple representation of the grain-boundary scattering model [96], electron scattering can be considered as the scattering on potential barriers that appear perpendicular to transport direction at a distance of the average grain size $\mathcal{D}$. When the electron encounters one grain boundary, the mfp can be reduced by factor of $\mathcal{T}$, where $\mathcal{T}$ is the transmission probability of electrons through the grain boundary. The number of times that an electron will have a collision event with a grain boundary along one mfp is $l_0/\mathcal{D}$, where l_0 is the mean-free path in absence of granularity. Thus, the final restricted effective mfp can be written as $l_{\mathrm{eff}} = l_0 \mathcal{T}^{l_0/\mathcal{D}}$. In case of this only mechanism, the effective resistivity can be given in the following way: $\rho_{\mathrm{eff}} = (3\pi^2)^{1/3}\hbar/(n_0^{2/3} e^2 l_{\mathrm{eff}})$, here, for simplicity, n_0 is taken as the carrier density of bulk material without crystal boundaries. To account this effect in the studied NbN films,

one needs to know what happens with intergrain barriers, the grain size, or point defects with increasing disorder. Thus, the fitting procedure with the grain boundary model [96] seems unreliable in determining the reasons for the reduced conductivity in our study. Meanwhile, one can expect a decrease in the effective grain size for NbN films deposited at lower $T_{\rm dep}$, as well as under excessive nitrogen partial pressure [80]. If one considers the fixed value of the transmission probability $\mathcal{T} \approx 0.15$, found for NbN films [47], the effective size of a crystalline grain $\mathcal{D}$ estimated from the resistivity falls within the range $a < \mathcal{D} < d$, where $d = 2.5$ nm is the film thickness and $a \approx 0.44$ nm is the lattice constant. However, this assumption requires further experimental verification. For instance, it would be very useful to check whether the grain size decreases with increasing disorder in NbN films by studying the evolution of the width of the x-ray diffraction peaks with disorder.

APPENDIX D: MAGNETOCONDUCTANCE

To derive τ_ϕ from the magnetoconductance at temperatures $T \geqslant T_c$, we fit data with the dimensionless change in magnetoconductance, which is given by expression

$$\delta G^{\rm QC} = G^{\rm QC}(B, T) - G^{\rm QC}(0, T), \tag{D1}$$

where $G^{\rm QC}(B, T)$ and $G^{\rm QC}(0, T)$ are a sum of four terms of quantum corrections to conductivity at finite and zero magnetic fields: the weak localization (WL), the Aslamazov-Larkin (AL) term, the density of states (DOS) contribution term, and Maki-Thomson (MT) term. The sum of these terms is given by the following expression [52,97–99]:

$$\begin{aligned} G^{\rm QC}(B,T) &= \underbrace{\frac{\pi^2\epsilon}{4h^2}\left[\psi\left(\frac{1}{2}+\frac{\epsilon}{2h}\right)-\psi\left(1+\frac{\epsilon}{2h}\right)+\frac{h}{\epsilon}\right]}_{\rm AL} \\ &\underbrace{-\frac{28\zeta(3)}{\pi^2}\left[\ln\left(\frac{1}{2h}\right)-\psi\left(\frac{1}{2}+\frac{\epsilon}{2h}\right)\right]}_{\rm DOS} \\ &\underbrace{-\beta_{\rm MT}(T,\tau_\phi)\left[\psi\left(\frac{1}{2}+\frac{B_\phi}{B}\right)-\psi\left(\frac{1}{2}+\frac{B_\phi}{B}\frac{\epsilon}{\gamma_\phi}\right)\right]}_{\rm MT} \\ &\underbrace{+\frac{3}{2}\psi\left(\frac{1}{2}+\frac{B_2}{B}\right)-\psi\left(\frac{1}{2}+\frac{B_1}{B}\right)-\frac{1}{2}\psi\left(\frac{1}{2}+\frac{B_3}{B}\right)}_{\rm WL}, \end{aligned} \tag{D1a}$$

where $\psi(x)$ is digamma function, $h = 0.69B/B_{c2}(0)$ and $\epsilon = \ln(T/T_c)$, $\gamma_\phi = \pi\hbar/(8k_BT\tau_\phi)$, $B_1 = B_0 + B_{\rm so}$, $B_2 = B_\phi + 4B_{\rm so}/3 + 2B_s/3$, and $B_3 = B_\phi + 2B_s$. The characteristic fields are defined as $B_0 = \hbar/(4eD\tau)$, $B_{\rm so} = \hbar/(4eD\tau_{\rm so})$, and $B_\phi = \hbar/(4eD\tau_\phi)$, where τ, $\tau_{\rm so}$, and τ_ϕ are the relaxation time for elastic, spin-orbit, and phase-breaking scattering, respectively. The spin-orbit time can be roughly estimated using $\tau_{\rm so} = \tau(\alpha Z)^{-4} \approx 0.01$–$0.1$ ps, where τ is the elastic scattering time, α is the fine structure constant, and Z is the effective atomic number of material ($Z_{\rm NbN} \approx 24$). The magnetic scattering is assumed to negligible ($B_s = 0$) since the samples are covered with a protective layer. The coefficient in MT term is given as [98]

$$\beta_{\rm MT}(T,\tau_\phi) = \frac{\pi^2}{4}\sum_i (-1)^i \Gamma(|i|) - \sum_{i\geqslant 0}\Gamma''(2i+1), \tag{D1b}$$

where $i = 0, \pm1, \pm2\ldots$ and $\Gamma^{-1}(|i|) = \epsilon + \psi(1/2 + |i|/2) - \psi(1/2) - \psi'(1/2 + |i|/2)2\gamma_\phi/\pi^2$. Note that AL and DOS terms in Eq. (D1a) are asymptotics for low temperatures $\epsilon \ll 1$. Nevertheless, the derivation of τ_ϕ at high temperatures does not depend on presence of AL and DOS terms in Eq. (D1a).

In the limit of zero magnetic field, Eq. (D1a) with adding the e-e contribution [6] can be transformed to

$$\begin{aligned} G^{\rm QC}(0,T) = &\underbrace{\frac{\pi^2}{8\epsilon}}_{\rm AL} + \underbrace{\frac{28\zeta(3)}{\pi^2}\ln(\epsilon)}_{\rm DOS} + \underbrace{\beta_{\rm MT}(T,\tau_\phi)\ln\left(\epsilon/\gamma_\phi\right)}_{\rm MT} \\ &\underbrace{+\ln\left(\frac{B_2}{B_1}\right)+\frac{1}{2}\ln\left(\frac{B_2}{B_3}\right)}_{\rm WL} + \underbrace{\ln\left(\frac{kT\tau}{\hbar}\right)}_{\rm e\text{-}e}. \end{aligned} \tag{D1c}$$

Equation (D1c) can be used for fitting $R_s(T)$ curve at low temperatures $\epsilon \ll 1$. To fit high-T part of resistance we replace the AL and DOS terms with $2.32/\epsilon^3$ and $-\pi^4/96\epsilon^2$ asymptotics, respectively [97].

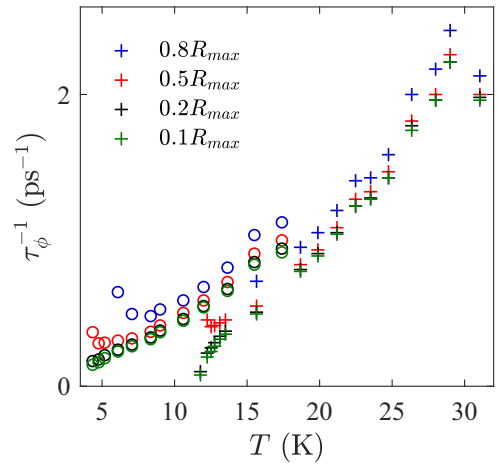

FIG. 9. Temperature dependencies of the phase-breaking time $\tau_\phi(T)$ estimated at different points of the superconducting resistive transition, which correspond to different set points of T_c ($0.8R_{\rm max}$, $0.5R_{\rm max}$, $0.2R_{\rm max}$, and $0.1R_{\rm max}$). The data are presented for two samples: s1 (cross-shaped symbols) and s6 (round symbols).

APPENDIX E: INFLUENCE OF THE CHOICE OF T_c ON ESTIMATES OF τ_ϕ

To fit the experimental data for the magnetoconductance with the fluctuation spectroscopy, we use T_c as a fitting parameter. Nominally, the critical temperature T_c in our study is determined as the temperature at which $R_s = R_{\rm max}/2$. Figure 9 shows that the choice of T_c at different set points barely affects the extracted phase-breaking time τ_ϕ.

APPENDIX F: ESTIMATE OF THE PHONON ESCAPE TIME

The characteristic phonon escape time can be found as $\tau_{esc} = (C_{ph}d)/(4\Sigma_{2D}T^3)$ [100], where $C_{ph} = 12\pi^4/5k_Ba^{-3}(T/\theta_D)^3$ is the phonon heat capacity in the 3D Debye model and Σ_{2D} is the heat flow rate limited by the Kapitza resistance. Taking into account the experimentally determined cooling rate for NbN-Al_2O_3 interface $\Sigma_{2D} \sim 120$ WK^{-4} m^{-2} [100], $d = 2.5$ nm, $a = 0.44$ nm, and $\theta_D = 116$ K, we obtain $\tau_{esc} \approx 120$ ps.

[1] B. Sacépé, M. Feigel'man, and T. M. Klapwijk, Quantum breakdown of superconductivity in low-dimensional materials, Nat. Phys. **16**, 734 (2020).

[2] A. D. Semenov, Superconducting nanostrip single-photon detectors some fundamental aspects in detection mechanism, technology and performance, Supercond. Sci. Technol. **34**, 054002 (2021).

[3] A. Shurakov, Y. Lobanov, and G. Goltsman, Superconducting hot-electron bolometer: From the discovery of hot-electron phenomena to practical applications, Supercond. Sci. Technol. **29**, 023001 (2016).

[4] J. Zmuidzinas, Superconducting microresonators: Physics and applications, Annu. Rev. Condens. Matter Phys. **3**, 169 (2012).

[5] P. J. de Visser, S. A. H. de Rooij, V. Murugesan, D. J. Thoen, and J. J. A. Baselmans, Phonon-Trapping-Enhanced Energy Resolution in Superconducting Single-Photon Detectors, Phys. Rev. Appl. **16**, 034051 (2021).

[6] B. Altshuler and A. Aronov, in *Electron–Electron Interactions in Disordered Systems* (Elsevier, Amsterdam, 1985), pp. 1–153.

[7] A. Anthore, F. Pierre, H. Pothier, and D. Esteve, Magnetic-Field-Dependent Quasiparticle Energy Relaxation in Mesoscopic Wires, Phys. Rev. Lett. **90**, 076806 (2003).

[8] B. Huard, A. Anthore, N. O. Birge, H. Pothier, and D. Esteve, Effect of Magnetic Impurities on Energy Exchange between Electrons, Phys. Rev. Lett. **95**, 036802 (2005).

[9] A. Schmid, Electron-phonon interaction in an impure metal, Z. Phys. **259**, 421 (1973).

[10] A. Sergeev and V. Mitin, Electron-phonon interaction in disordered conductors: Static and vibrating scattering potentials, Phys. Rev. B **61**, 6041 (2000).

[11] A. Shtyk and M. Feigel'man, Ultrasonic attenuation via energy diffusion channel in disordered conductors, Phys. Rev. B **92**, 195101 (2015).

[12] M. E. Gershenson, D. Gong, T. Sato, B. S. Karasik, and A. V. Sergeev, Millisecond electron–phonon relaxation in ultrathin disordered metal films at millikelvin temperatures, Appl. Phys. Lett. **79**, 2049 (2001).

[13] J. J. Lin and J. P. Bird, Recent experimental studies of electron dephasing in metal and semiconductor mesoscopic structures, J. Phys.: Condens. Matter **14**, R501 (2002).

[14] J. T. Karvonen, L. J. Taskinen, and I. J. Maasilta, Observation of disorder-induced weakening of electron-phonon interaction in thin noble-metal films, Phys. Rev. B **72**, 012302 (2005).

[15] S. P. Chockalingam, M. Chand, J. Jesudasan, V. Tripathi, and P. Raychaudhuri, Superconducting properties and Hall effect of epitaxial NbN thin films, Phys. Rev. B **77**, 214503 (2008).

[16] M. Chand, G. Saraswat, A. Kamlapure, M. Mondal, S. Kumar, J. Jesudasan, V. Bagwe, L. Benfatto, V. Tripathi, and P. Raychaudhuri, Phase diagram of the strongly disordered *s*-wave superconductor NbN close to the metal-insulator transition, Phys. Rev. B **85**, 014508 (2012).

[17] P. I. Zolotov, A. V. Semenov, A. V. Divochiy, G. N. Goltsman, N. R. Romanov, and T. M. Klapwijk, Dependence of photon detection efficiency on normal-state sheet resistance in marginally superconducting films of NbN, IEEE Trans. Appl. Supercond. **31**, 1 (2021).

[18] G. N. Gol'tsman, O. Okunev, G. Chulkova, A. Lipatov, A. Semenov, K. Smirnov, B. Voronov, A. Dzardanov, C. Williams, and R. Sobolewski, Picosecond superconducting single-photon optical detector, Appl. Phys. Lett. **79**, 705 (2001).

[19] A. Divochiy, M. Misiaszek, Y. Vakhtomin, P. Morozov, K. Smirnov, P. Zolotov, and P. Kolenderski, Single photon detection system for visible and infrared spectrum range, Opt. Lett. **43**, 6085 (2018).

[20] I. Tretyakov, S. Ryabchun, M. Finkel, A. Maslennikova, N. Kaurova, A. Lobastova, B. Voronov, and G. Gol'tsman, Low noise and wide bandwidth of NbN hot-electron bolometer mixers, Appl. Phys. Lett. **98**, 033507 (2011).

[21] A. J. Annunziata, D. F. Santavicca, L. Frunzio, G. Catelani, M. J. Rooks, A. Frydman, and D. E. Prober, Tunable superconducting nanoinductors, Nanotechnology **21**, 445202 (2010).

[22] D. Niepce, J. Burnett, and J. Bylander, High Kinetic Inductance NbN Nanowire Superinductors, Phys. Rev. Appl. **11**, 044014 (2019).

[23] J. T. Peltonen, O. V. Astafiev, Y. P. Korneeva, B. M. Voronov, A. A. Korneev, I. M. Charaev, A. V. Semenov, G. N. Golt'sman, L. B. Ioffe, T. M. Klapwijk, and J. S. Tsai, Coherent flux tunneling through NbN nanowires, Phys. Rev. B **88**, 220506(R) (2013).

[24] K. Y. Arutyunov, A. Ramos-Álvarez, A. V. Semenov, Y. P. Korneeva, P. P. An, A. A. Korneev, A. Murphy, A. Bezryadin, and G. N. Gol'tsman, Superconductivity in highly disordered NbN nanowires, Nanotechnology **27**, 47LT02 (2016).

[25] J. T. Peltonen, Z. H. Peng, Y. P. Korneeva, B. M. Voronov, A. A. Korneev, A. V. Semenov, G. N. Gol'tsman, J. S. Tsai, and O. V. Astafiev, Coherent dynamics and decoherence in a superconducting weak link, Phys. Rev. B **94**, 180508(R) (2016).

[26] N. G. N. Constantino, M. S. Anwar, O. W. Kennedy, M. Dang, P. A. Warburton, and J. C. Fenton, Emergence of quantum phase-slip behaviour in superconducting NbN nanowires: DC electrical transport and fabrication technologies, Nanomaterials **8**, 442 (2018).

[27] S. E. de Graaf, S. T. Skacel, T. Hönigl-Decrinis, R. Shaikhaidarov, H. Rotzinger, S. Linzen, M. Ziegler, U. Hübner, H.-G. Meyer, V. Antonov, E. Il'ichev, A. V. Ustinov, A. Y. Tzalenchuk, and O. V. Astafiev, Charge quantum interference device, Nat. Phys. **14**, 590 (2018).

[28] R. S. Shaikhaidarov, K. H. Kim, J. W. Dunstan, I. V. Antonov, S. Linzen, M. Ziegler, D. S. Golubev, V. N. Antonov, E. V. Il'ichev, and O. V. Astafiev, Quantized current steps due to the

a.c. coherent quantum phase-slip effect, Nature (London) **608**, 45 (2022).

[29] Y. P. Gousev, G. N. Gol'tsman, A. D. Semenov, E. M. Gershenzon, R. S. Nebosis, M. A. Heusinger, and K. F. Renk, Broadband ultrafast superconducting NbN detector for electromagnetic radiation, J. Appl. Phys. **75**, 3695 (1994).

[30] M. Mondal, S. Kumar, M. Chand, A. Kamlapure, G. Saraswat, G. Seibold, L. Benfatto, and P. Raychaudhuri, Role of the Vortex-Core Energy on the Berezinskii-Kosterlitz-Thouless Transition in Thin Films of NbN, Phys. Rev. Lett. **107**, 217003 (2011).

[31] C. Delacour, B. Pannetier, J.-C. Villegier, and V. Bouchiat, Quantum and thermal phase slips in superconducting niobium nitride (NbN) ultrathin crystalline nanowire: Application to single photon detection, Nano Lett. **12**, 3501 (2012).

[32] M. Mondal, A. Kamlapure, S. C. Ganguli, J. Jesudasan, V. Bagwe, L. Benfatto, and P. Raychaudhuri, Enhancement of the finite-frequency superfluid response in the pseudogap regime of strongly disordered superconducting films, Sci. Rep. **3**, 1357 (2013).

[33] Y. Noat, V. Cherkez, C. Brun, T. Cren, C. Carbillet, F. Debontridder, K. Ilin, M. Siegel, A. Semenov, H.-W. Hübers, and D. Roditchev, Unconventional superconductivity in ultrathin superconducting NbN films studied by scanning tunneling spectroscopy, Phys. Rev. B **88**, 014503 (2013).

[34] C. Carbillet, V. Cherkez, M. A. Skvortsov, M. V. Feigel'man, F. Debontridder, L. B. Ioffe, V. S. Stolyarov, K. Ilin, M. Siegel, D. Roditchev, T. Cren, and C. Brun, Spectroscopic evidence for strong correlations between local superconducting gap and local Altshuler-Aronov density of states suppression in ultrathin NbN films, Phys. Rev. B **102**, 024504 (2020).

[35] K. S. Il'in, M. Lindgren, M. Currie, A. D. Semenov, G. N. Gol'tsman, R. Sobolewski, S. I. Cherednichenko, and E. M. Gershenzon, Picosecond hot-electron energy relaxation in NbN superconducting photodetectors, Appl. Phys. Lett. **76**, 2752 (2000).

[36] J. Zhang, W. Słysz, A. Pearlman, A. Verevkin, R. Sobolewski, O. Okunev, G. Chulkova, and G. N. Gol'tsman, Time delay of resistive-state formation in superconducting stripes excited by single optical photons, Phys. Rev. B **67**, 132508 (2003).

[37] S.-Z. Lin, O. Ayala-Valenzuela, R. D. McDonald, L. N. Bulaevskii, T. G. Holesinger, F. Ronning, N. R. Weisse-Bernstein, T. L. Williamson, A. H. Mueller, M. A. Hoffbauer, M. W. Rabin, and M. J. Graf, Characterization of the thin-film NbN superconductor for single-photon detection by transport measurements, Phys. Rev. B **87**, 184507 (2013).

[38] L. Zhang, L. You, X. Yang, J. Wu, C. Lv, Q. Guo, W. Zhang, H. Li, W. Peng, Z. Wang, and X. Xie, Hotspot relaxation time of NbN superconducting nanowire single-photon detectors on various substrates, Sci. Rep. **8**, 1486 (2018).

[39] M. Sidorova, A. Semenov, H.-W. Hübers, K. Ilin, M. Siegel, I. Charaev, M. Moshkova, N. Kaurova, G. N. Goltsman, X. Zhang, and A. Schilling, Electron energy relaxation in disordered superconducting NbN films, Phys. Rev. B **102**, 054501 (2020).

[40] L. Zhang, L. You, W. Peng, and Z. Wang, Quasiparticle scattering time in NbN superconducting thin films, Phys. C (Amsterdam) **579**, 1353773 (2020).

[41] S. Linzen, M. Ziegler, O. V. Astafiev, M. Schmelz, U. Hübner, M. Diegel, E. Il'ichev, and H.-G. Meyer, Structural and electrical properties of ultrathin niobium nitride films grown by atomic layer deposition, Supercond. Sci. Technol. **30**, 035010 (2017).

[42] E. Knehr, M. Ziegler, S. Linzen, K. Ilin, P. Schanz, J. Plentz, M. Diegel, H. Schmidt, E. Il'ichev, and M. Siegel, Wafer-level uniformity of atomic-layer-deposited niobium nitride thin films for quantum devices, J. Vac. Sci. Technol. A: Vac. Surf. **39**, 052401 (2021).

[43] B. Shinozaki, S. Ezaki, T. Odou, T. Asano, and K. Makise, Anomalous electron inelastic scattering rate probed via superconducting fluctuation in epitaxial NbN thin films, Phys. C (Amsterdam) **567**, 1353547 (2019).

[44] M. Sidorova, A. D. Semenov, H.-W. Hübers, S. Gyger, S. Steinhauer, X. Zhang, and A. Schilling, Magnetoconductance and photoresponse properties of disordered NbTiN films, Phys. Rev. B **104**, 184514 (2021).

[45] A. Nigro, G. Nobile, M. G. Rubino, and R. Vaglio, Electrical resistivity of polycrystalline niobium nitride films, Phys. Rev. B **37**, 3970 (1988).

[46] J. Tyan and J. T. Lue, Grain boundary scattering in the normal state resistivity of superconducting NbN thin films, J. Appl. Phys. **75**, 325 (1994).

[47] K. Senapati, N. K. Pandey, R. Nagar, and R. C. Budhani, Normal-state transport and vortex dynamics in thin films of two structural polymorphs of superconducting nbn, Phys. Rev. B **74**, 104514 (2006).

[48] L. Benfatto, C. Castellani, and T. Giamarchi, Broadening of the Berezinskii-Kosterlitz-Thouless superconducting transition by inhomogeneity and finite-size effects, Phys. Rev. B **80**, 214506 (2009).

[49] S. Caprara, M. Grilli, L. Benfatto, and C. Castellani, Effective medium theory for superconducting layers: A systematic analysis including space correlation effects, Phys. Rev. B **84**, 014514 (2011).

[50] T. I. Baturina, S. V. Postolova, A. Y. Mironov, A. Glatz, M. R. Baklanov, and V. M. Vinokur, Superconducting phase transitions in ultrathin TiN films, Europhys. Lett. **97**, 17012 (2012).

[51] M. Mondal, M. Chand, A. Kamlapure, J. Jesudasan, V. C. Bagwe, S. Kumar, G. Saraswat, V. Tripathi, and P. Raychaudhuri, Phase diagram and upper critical field of homogeneously disordered epitaxial 3-dimensional NbN films, J. Supercond. Nov. Magn. **24**, 341 (2011).

[52] A. A. Varlamov, A. Galda, and A. Glatz, Fluctuation spectroscopy: From Rayleigh-Jeans waves to Abrikosov vortex clusters, Rev. Mod. Phys. **90**, 015009 (2018).

[53] A. Abrikosov and L. Gor'kov, Contribution to the theory of superconducting alloys with paramagnetic impurities, Sov. Phys.–JETP **12**, 1243 (1961).

[54] E. Müller-Hartmann and J. Zittartz, Kondo Effect in Superconductors, Phys. Rev. Lett. **26**, 428 (1971).

[55] Y. V. Fominov, M. Houzet, and L. I. Glazman, Surface impedance of superconductors with weak magnetic impurities, Phys. Rev. B **84**, 224517 (2011).

[56] A. Rogachev, A. T. Bollinger, and A. Bezryadin, Influence of High Magnetic Fields on the Superconducting Transition of One-Dimensional Nb and MoGe Nanowires, Phys. Rev. Lett. **94**, 017004 (2005).

[57] P. Kumar, S. Sendelbach, M. A. Beck, J. W. Freeland, Z. Wang, H. Wang, C. C. Yu, R. Q. Wu, D. P. Pappas, and R. McDermott, Origin and Reduction of $1/f$ Magnetic Flux Noise in Superconducting Devices, Phys. Rev. Appl. **6**, 041001(R) (2016).

[58] A. S. Samsonova, P. I. Zolotov, E. M. Baeva, A. I. Lomakin, N. A. Titova, A. I. Kardakova, and G. N. Goltsman, Signatures of surface magnetic disorder in niobium films, IEEE Trans. Appl. Supercond. **31**, 1 (2021).

[59] E. Sheridan, T. F. Harrelson, E. Sivonxay, K. A. Persson, M. V. P. Altoé, I. Siddiqi, D. F. Ogletree, D. I. Santiago, and S. M. Griffin, Microscopic theory of magnetic disorder-induced decoherence in superconducting Nb films, arXiv:2111.11684.

[60] W. Brenig, M.-c. Chang, E. Abrahams, and P. Wölfle, Inelastic scattering time above the superconductivity transition in two dimensions: Dependence on disorder and magnetic field, Phys. Rev. B **31**, 7001 (1985).

[61] M. Khodas and A. M. Finkel'stein, Hall coefficient in an interacting electron gas, Phys. Rev. B **68**, 155114 (2003).

[62] The dephasing time due to e-ph scattering is identical to the single-particle e-ph scattering time $\tau_{\text{e-ph}}$. The e-ph energy relaxation time, measured by the AMAR method, is proportional to the $\tau_{\text{e-ph}}$ with a proportionality coefficient, which depends on the exponent p: it is about 0.6 for $p = 2.0$.

[63] A. Pippard, CXXII. Ultrasonic attenuation in metals, Philos. Mag. **46**, 1104 (1955).

[64] J. Rammer and A. Schmid, Destruction of phase coherence by electron-phonon interactions in disordered conductors, Phys. Rev. B **34**, 1352 (1986).

[65] V. F. Gantmakher, The experimental study of electron-phonon scattering in metals, Rep. Prog. Phys. **37**, 317 (1974).

[66] F. C. Wellstood, C. Urbina, and J. Clarke, Hot-electron effects in metals, Phys. Rev. B **49**, 5942 (1994).

[67] M. Prunnila, P. Kivinen, A. Savin, P. Törmä, and J. Ahopelto, Intervalley-Scattering-Induced Electron-Phonon Energy Relaxation in Many-Valley Semiconductors at Low Temperatures, Phys. Rev. Lett. **95**, 206602 (2005).

[68] S.-X. Qu, A. N. Cleland, and M. R. Geller, Hot electrons in low-dimensional phonon systems, Phys. Rev. B **72**, 224301 (2005).

[69] A. Sergeev, M. Y. Reizer, and V. Mitin, Deformation Electron-Phonon Coupling in Disordered Semiconductors and Nanostructures, Phys. Rev. Lett. **94**, 136602 (2005).

[70] S. Ono, Low-temperature electron-phonon relaxation in Cu and Ag thin films, Phys. Rev. B **101**, 201404(R) (2020).

[71] C. Pethick and H. Smith, Relaxation and collective motion in superconductors: A two-fluid description, Ann. Phys. **119**, 133 (1979).

[72] K. R. Babu and G.-Y. Guo, Electron-phonon coupling, superconductivity, and nontrivial band topology in NbN polytypes, Phys. Rev. B **99**, 104508 (2019).

[73] R. Yang, Z. Zhao, F. Wu, Q. Wei, and M. Xue, Study on structural, mechanical, electronic properties and debye temperature of four NbN structures, Comput. Theor. Chem. **1196**, 113113 (2021).

[74] S. B. Kaplan, Acoustic matching of superconducting films to substrates, J. Low Temp. Phys. **37**, 343 (1979).

[75] M. V. Sidorova, A. G. Kozorezov, A. V. Semenov, Y. P. Korneeva, M. Y. Mikhailov, A. Y. Devizenko, A. A. Korneev, G. M. Chulkova, and G. N. Goltsman, Nonbolometric bottleneck in electron-phonon relaxation in ultrathin WSi films, Phys. Rev. B **97**, 184512 (2018).

[76] K. S. Il'in, N. G. Ptitsina, A. V. Sergeev, G. N. Gol'tsman, E. M. Gershenzon, B. S. Karasik, E. V. Pechen, and S. I. Krasnosvobodtsev, Interrelation of resistivity and inelastic electron-phonon scattering rate in impure NbC films, Phys. Rev. B **57**, 15623 (1998).

[77] D. Y. Vodolazov, Single-Photon Detection by a Dirty Current-Carrying Superconducting Strip Based on the Kinetic-Equation Approach, Phys. Rev. Appl. **7**, 034014 (2017).

[78] M. Hofherr, D. Rall, K. Ilin, M. Siegel, A. Semenov, H.-W. Hübers, and N. A. Gippius, Intrinsic detection efficiency of superconducting nanowire single-photon detectors with different thicknesses, J. Appl. Phys. **108**, 014507 (2010).

[79] Y. P. Korneeva, N. N. Manova, M. A. Dryazgov, N. O. Simonov, P. I. Zolotov, and A. A. Korneev, Influence of sheet resistance and strip width on the detection efficiency saturation in micron-wide superconducting strips and large-area meanders, Supercond. Sci. Technol. **34**, 084001 (2021).

[80] A. H. Farha, Investigation of NbNx thin films and nanoparticles grown by pulsed laser deposition and thermal diffusion, Ph.D. thesis, Old Dominion University, Norfolk, 2013.

[81] E. C. Ethridge, S. C. Erwin, and W. E. Pickett, Nb_4N_3: Polymorphism in crystalline niobium nitrides, Phys. Rev. B **53**, 12563 (1996).

[82] Y. Pan, H. Zhou, L. Zhang, H. Li, Y. Tang, H. Yu, M. Si, L. You, and Z. Wang, Superconducting nanowire single-photon detector made of ultrathin γ-Nb_4N_3 film for mid-infrared wavelengths, Supercond. Sci. Technol. **34**, 074001 (2021).

[83] B. Scheerer, *Preparation of NbN Single Crystals* (Karlsruhe, Kernforschungszentrum Karlsruhe, 1979).

[84] A. V. Lubenchenko, A. A. Batrakov, A. B. Pavolotsky, O. I. Lubenchenko, and D. A. Ivanov, XPS study of multilayer multicomponent films, Appl. Surf. Sci. **427**, 711 (2018).

[85] M. D. Soldatenkova, A. D. Triznova, E. M. Baeva, P. I. Zolotov, A. I. Lomakin, A. I. Kardakova, and G. N. Goltsman, Normal-state transport in superconducting NbN films on r-cut sapphire, J. Phys.: Conf. Ser. **2086**, 012212 (2021).

[86] M. Benkahoul, Niobium nitride based thin films deposited by dc reactive magnetron sputtering: NbN, NbSiN and NbAlN, Ph.D. thesis, Université de Constantine, Lausanne, 2005.

[87] A. Finkel'stein, Suppression of superconductivity in homogeneously disordered systems, Phys. B (Amsterdam) **197**, 636 (1994).

[88] D. S. Antonenko and M. Skvortsov, Suppression of superconductivity in disordered films: Interplay of two-dimensional diffusion and three-dimensional ballistics, JEPT Lett. **112**, 428 (2020).

[89] P. Raychaudhuri and S. Dutta, Phase fluctuations in conventional superconductors, J. Phys.: Condens. Matter **34**, 083001 (2022).

[90] S. Dutta, P. Raychaudhuri, S. S. Mandal, and T. V. Ramakrishnan, Superfluid density in conventional superconductors: From clean to strongly disordered, J. Phys.: Condens. Matter **34**, 335601 (2022).

[91] M. Chand, A. Mishra, Y. M. Xiong, A. Kamlapure, S. P. Chockalingam, J. Jesudasan, V. Bagwe, M. Mondal, P. W. Adams, V. Tripathi, and P. Raychaudhuri, Temperature dependence of resistivity and Hall coefficient in strongly disordered NbN thin films, Phys. Rev. B **80**, 134514 (2009).

[92] C. Kittel, *Introduction to Solid State Physics*, 8th ed. (Wiley, New York, 2004).

[93] A. Semenov, B. Günther, U. Böttger, H.-W. Hübers, H. Bartolf, A. Engel, A. Schilling, K. Ilin, M. Siegel, R. Schneider, D. Gerthsen, and N. A. Gippius, Optical and transport properties of ultrathin NbN films and nanostructures, Phys. Rev. B **80**, 054510 (2009).

[94] G. Oya and Y. Onodera, Transition temperatures and crystal structures of single-crystal and polycrystalline NbN_x films, J. Appl. Phys. **45**, 1389 (1974).

[95] A. F. Mayadas and M. Shatzkes, Electrical-resistivity model for polycrystalline films: The case of arbitrary reflection at external surfaces, Phys. Rev. B **1**, 1382 (1970).

[96] G. Reiss, J. Vancea, and H. Hoffmann, Grain-Boundary Resistance in Polycrystalline Metals, Phys. Rev. Lett. **56**, 2100 (1986).

[97] A. Glatz, A. A. Varlamov, and V. M. Vinokur, Fluctuation spectroscopy of disordered two-dimensional superconductors, Phys. Rev. B **84**, 104510 (2011).

[98] J. M. B. Lopes dos Santos and E. Abrahams, Superconducting fluctuation conductivity in a magnetic field in two dimensions, Phys. Rev. B **31**, 172 (1985).

[99] R. Rosenbaum, Superconducting fluctuations and magnetoconductance measurements of thin films in parallel magnetic fields, Phys. Rev. B **32**, 2190 (1985).

[100] A. Dane, J. Allmaras, D. Zhu, M. Onen, M. Colangelo, R. Baghdadi, J.-L. Tambasco, Y. Morimoto, I. E. Forno, I. Charaev, Q. Zhao, M. Skvortsov, A. Kozorezov, and K. K. Berggren, Self-heating hotspots in superconducting nanowires cooled by phonon black-body radiation, Nat. Commun. **13**, 5429 (2022).